Geometric Optics: Spherical and Chromatic Aberration

James Cowley
Department of Physics and Astronomy
University College London

22 March 2013

Abstract: A computer model is used to simulate the properties of variously shaped converging and diverging lenses and to examine how the spherical aberration produced by different kinds of converging lens varies with the dimensions of the lens. It is verified that thinner lenses produce less significant spherical aberration for all shapes modelled, and specific dimensional recommendations are made for reducing spherical aberration in asymmetrical biconvex lenses, concave positive menisci, plano-convex and convex-planar lenses. The comatic aberrations (coma) produced by these lenses are also plotted and hence their natures determined. Chromatic aberration is simulated and measured in different converging lenses, and an achromatic Clark doublet comprised of a borosilicate crown glass positive lens and a flint glass negative lens is examined to determine the separation distance of the two lenses which optimises the doublet's achromatism. The modelled flint glass lens is then gradually flattened to simulate a Littrow doublet, which is shown to be less effective at reducing chromatic aberrations than the Clark doublet.

Background

In the field of optics, the surfaces of lenses are often described in terms of spheres (or, in 2 dimensions, circles). Figure 1 illustrates how a variety of lenses can be constructed in this manner.

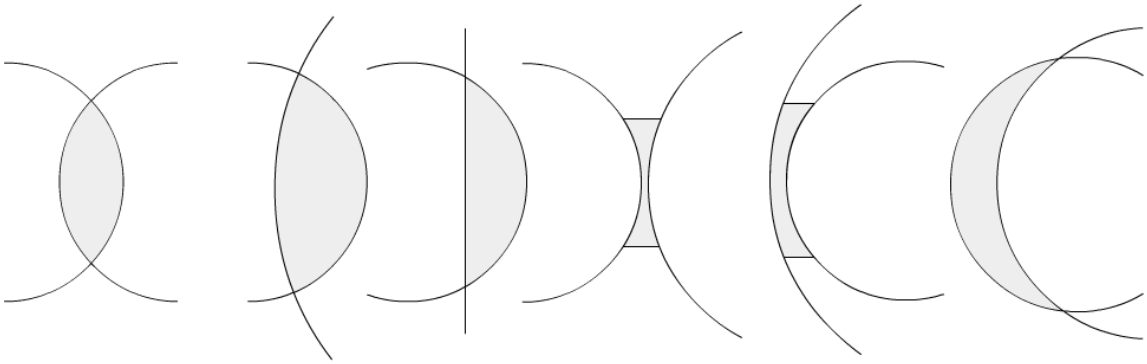

Figure 1: Different types of lens constructed from different combinations of circles. The lens types are, from left to right: symmetrical biconvex, asymmetrical biconvex, plano-convex, asymmetrical biconcave, negative meniscus and convex positive meniscus. In the case of the plano-convex lens, the arc of an extremely large circle is used to approximate the flat side.

This is one of several assumptions which simplify results during the treatment of lenses. Additionally, assuming that lenses are thin and that the glass out of which they are made is non-dispersive allows the derivation of the lens maker's equation:

$$\frac{1}{u}+\frac{1}{v}=\frac{1}{f} \tag{1}$$

Where u and v are the distances from the lens to the object and image respectively, and f is the focal length of the lens. In reality, lenses have non-negligible thickness, and the refractive index of glass varies for light of different frequencies (leading to chromatic aberrations in images). The result of these additional factors is illustrated in Figure 2.

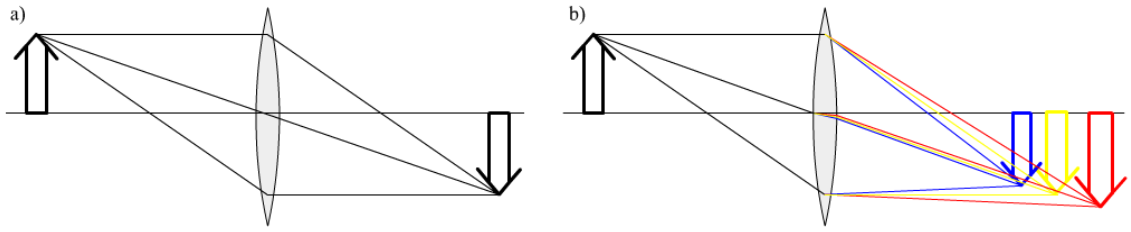

Figure 2: (a) The simplified behaviour of a lens governed by the lens maker's equation. The lens is assumed to be thin (so the rays pass straight through the centre) and made of non-dispersive achromatic glass (so all frequencies are refracted the same amount). (b) The behaviour of a lens in reality. The light rays are refracted when passing through the centre, and higher frequencies are refracted more, causing the blue rays to focus closer to the lens than the other colours, and a chromatically aberrated image is formed.

Additionally, in a real lens, paraxial rays are not brought to the same focus, producing spherical aberrations, as illustrated in Figure 3, and parallel beams at an angle to the axis are brought to a focus at different heights above the axis, producing comatic aberrations (coma), as illustrated in Figure 4. The reduction of aberrations is necessary to make all light rays from an image focus as closely together as possible. Systems of lenses finely tuned to minimise spherical and chromatic aberrations (such as achromatic doublets) have applications ranging from everyday photography to billion-dollar space telescopes.

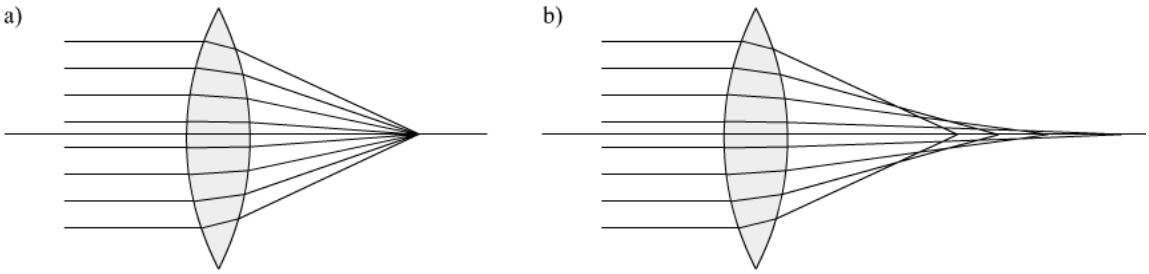

Figure 3: (a) The idealised focussing of paraxial light rays onto the same point. (b) In reality, rays at different distances from the axis are refracted to varying extents and focus at different points. The radius of the bright spot appearing on a screen placed at the first focus (i.e. the focus of the rays passing through the outer edge of the lens), defines the lateral spherical aberration.

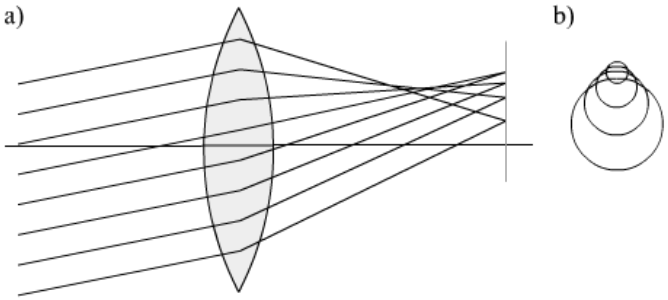

Figure 4: (a) Parallel light rays at an angle to the axis are focussed by the lens at different heights above the axis. (b) Comatic circles forming the image produced by this symmetrical biconvex lens. The "tail" points upward, away from the axis, so this is an example of negative coma.

Introduction

In order to examine the precise behaviour of a lens, it is convenient to use a computer model to calculate the path of an individual light ray exactly. The path of the ray as it approaches a lens can be defined by a starting point and initial angle of elevation from the lens axis, which can be converted to the equation of a straight line. This can then be solved simultaneously with the equation of a circle, using the radius and centre of curvature of the first face of the lens to find where the beam intersects that surface.

The angle of incidence can then be determined from the gradient of the line and that of the normal to the circle at the point of intersection, and hence the angle of refraction is determined by Snell's law:

$$\frac{\sin\theta_i}{\sin\theta_r} = \frac{n_2}{n_1} \tag{2}$$

Where θ_i and θ_r are the angles of incidence and refraction, and n_1 and n_2 are the refractive indices of the first and second media, respectively. This can then be repeated for the second boundary and the entire path of the beam through the lens can be found.

The model can then be used to demonstrate and measure the slight effects of spherical, comatic and chromatic aberrations for different lens shapes and combinations of lenses, thereby exploring ways to reduce these types of distortion.

Method

Wolfram *Mathematica* version 8.0 was used to construct a versatile model from a series of functions which could simulate different lens types and the path of light rays through them. Separate functions (a full record of which is available from the URL included in the section "Further Work") were written to calculate each stage of a light ray's path through a lens in chronological order:

1. Starting coordinates and angle of elevation determine the initial path of the light ray.
2. The point of intersection of this straight line and the surface of the lens, defined by its radius and centre of curvature, is then calculated.
3. The light ray's new angle of elevation is determined from Snell's law.
4. The previous 2 steps are repeated using the ray's point of entry into the lens and new angle of elevation in order to find its point of exit and its final angle of elevation.

Additional functions were written to plot the lenses and the light ray's path graphically, to illustrate the model's results. In order to test the model, it was first used to investigate the accuracy of the lens maker's equation. Figure 5 shows the result of this test.

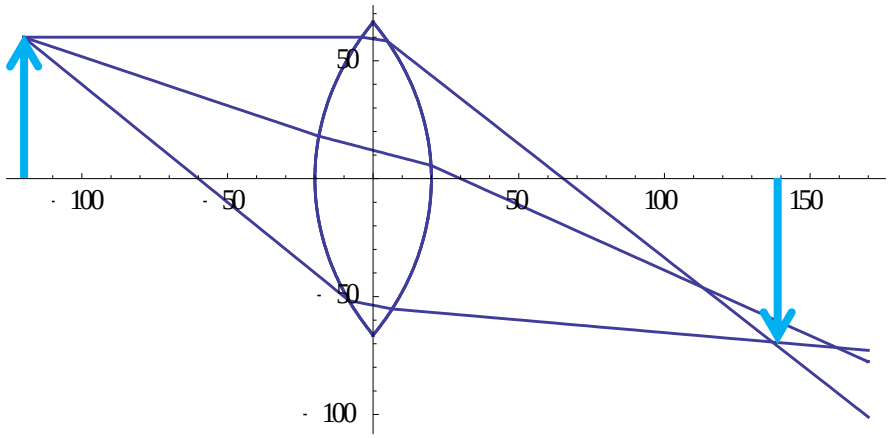

Figure 5: The modelled behaviour of (monochromatic) light from an object through a symmetrical biconvex in the situation illustrated in Figure 2 (with object and image arrows added manually).

The model matches the result given by the lens maker's equation reasonably closely, given that the latter is an approximation. In this instance, the object distance is 120 and the image distance is approximately 140, so the LHS of equation (1) becomes

$$\frac{1}{120} + \frac{1}{140} = \frac{13}{840}$$

The focal length is then

$$f = \frac{840}{13} \approx 65$$

The model agrees with this, as the focal length of the lens (taken to be the point where the top beam passes the *x*-axis) is approximately 65. As a further test of the model's capabilities, it was used to demonstrate the effect of monochromatic spherical aberrations in the case of a thin lens. The resulting behaviour is shown in Figure 6.

The model reproduced the result that thin lenses generate only very slight spherical aberration relative to their focal lengths. For the lens simulated in Figure 6, a screen placed at the focus gives a measured lateral spherical aberration of <0.8, i.e. <0.08% of the lens' focal length of 1000. As the thickness of the lenses was increased, so did the severity of the spherical aberration. Figure 7 shows the model's treatment of two thicker lenses, demonstrating that as thickness increases, spherical aberrations become more significant.

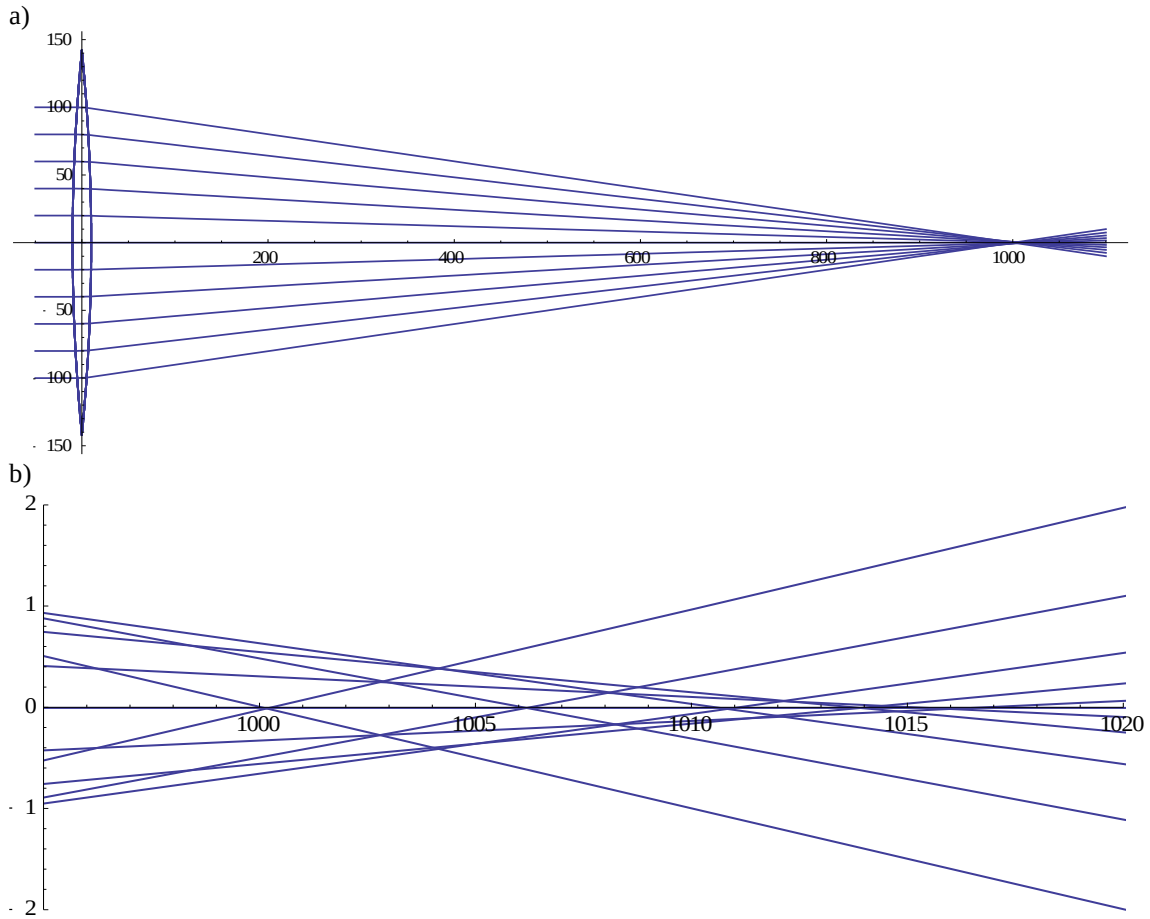

Figure 6: (a) The modelled result for a thin, symmetrical biconvex lens with radii of curvature ±1010 centred at ±1000, refracting paraxial rays at height intervals of 10. All beams converge far from the lens, making the aberration difficult to see at this scale. (b) A close-up of the rays' foci.

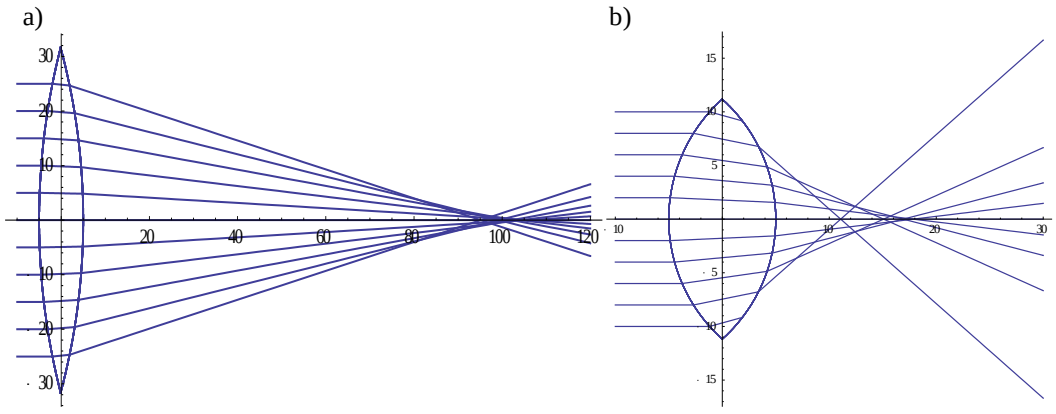

Figure 7: (a) Spherical aberration produced by fairly thick symmetrical biconvex lens with radii and centres of curvature ±105 and ±100. (b) Spherical aberration produced by a very thick symmetrical biconvex lens with radii and centres of curvature ±15 and ±10.

Spherical Aberrations

To quantitatively study the effect of changing the dimensions of the lens on spherical aberration, a function was defined to use 2 paraxial beams: the first placed at 60% of the distance between the axis and the edge of the lens, the second at half this height, as illustrated in Figure 8. The first beam is focused closer to the lens than the second, and the height of the second beam at that point (i.e. the radius of the spot of light on a screen at that point), is a measure of the aberration. As the system is symmetrical about the *x*-axis, beams through the lower half of the lens do not have to be considered to carry out this calculation.

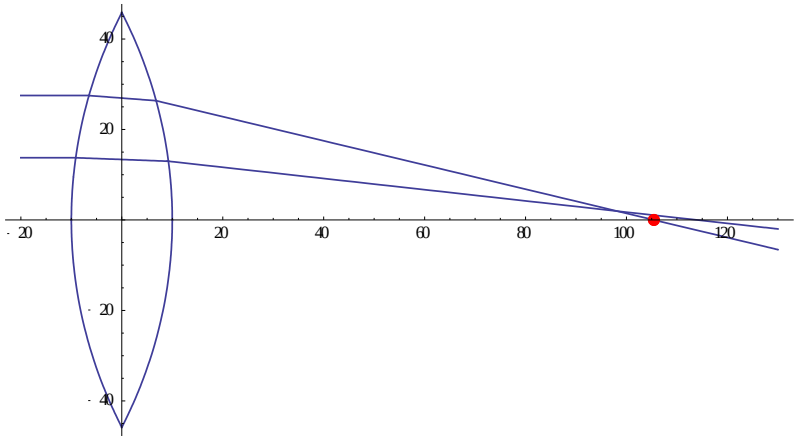

{ , 1.05405}

Figure 8: An example of the model measuring spherical aberration. The red point highlights the focus of the outer beam, and the number generated is the height of the other beam above the *x*-axis at this point.

It is to be noted that the value found in this manner is *not* the exact lateral spherical aberration, as that value is defined by the radius of the spot formed on a screen at the focus of a beam passing *through the very edge* of the lens. However, for ease of implementation, this reduced height was used in order to avoid some simulated beams passing through very rounded lenses near their edge and meeting the second lens boundary at an angle of incidence greater than the critical angle, thereby being totally internally reflected and not leaving the far side of the lens.

Comatic Aberrations (coma)

The functions which demonstrated spherical aberrations could be used without special alteration to determine the nature of the coma produced by different converging lenses, simply by setting a non-zero angle of elevation for a series of light rays at various heights entering each lens and then plotting the results.

Chromatic Aberrations

To demonstrate chromatic aberrations, the ray path plotting function was adjusted to accept an argument defining the colour of the beam, and then applied to the different refractive indices of glass at different frequencies to illustrate the chromatic aberrations produced by a single lens. The model's simulation of a biconvex borosilicate crown glass lens is shown in Figure 9.

In order to examine this phenomenon quantitatively and to investigate combinations of lenses (eventually forming an achromatic doublet), the plotting function was elaborated to enable it to determine the path of 2 light rays of different frequencies through 2 lenses of different compositions and different refractive indices. Since higher frequency light ray focusses closer to the lens, a convenient measurement of the chromatic aberration is the height of the other beam at the *x*-coordinate of this focus. Figure 10 illustrates the use of this function. A faster version of this function without its plotting capabilities was also created.

When investigating the properties of the Clark doublet, a borosilicate crown glass and flint glass were used. The refractive indices of the borosilicate crown for red, yellow and blue light (taken to be wavelengths 656.2186nm, 587.5618nm and 486.1327nm), were taken to be 1.50763, 1.51009 and 1.51566 respectively, and those for the flint glass were taken to be 1.61503, 1.62004, and 1.63208 respectively.

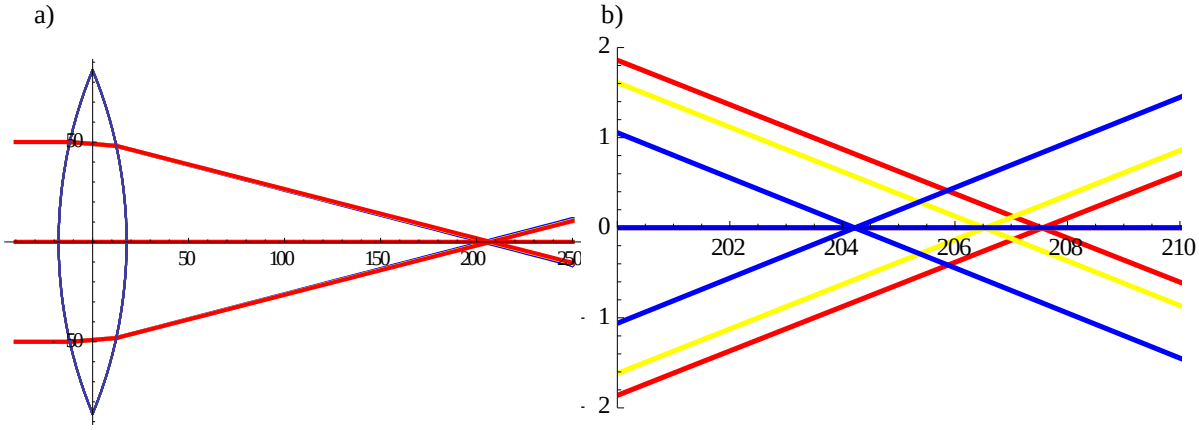

Figure 9: (a) Chromatic aberration in a symmetrical biconvex lens made of the borosilicate crown glass. (b) A close-up of the rays' foci.

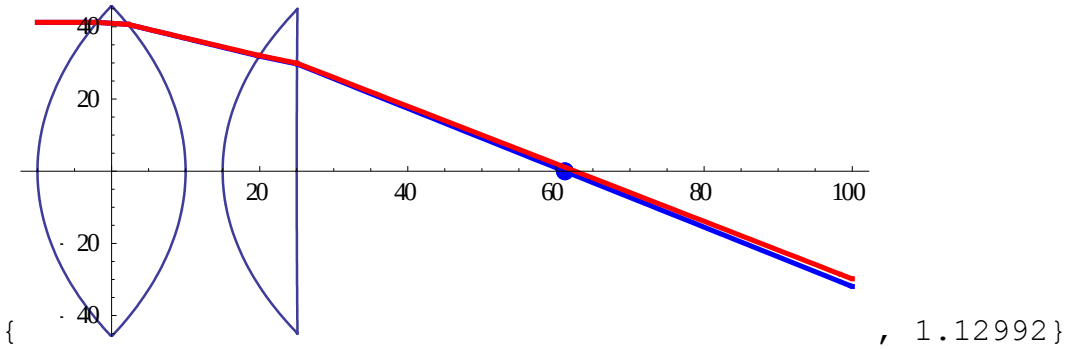

Figure 10: An example of the model measuring chromatic aberration through a pair of lenses both made of the same borosilicate crown glass as the lens in Figure 9. The blue point highlights the focus of the blue beam and the number generated is the height of the red beam above the *x*-axis at this point.

Results

Spherical Aberrations

A reduced form of the spherical aberration function (with its time-costly plotting capabilities removed, such that it only returned a numerical value for the aberration) was applied to a 2 dimensional variable space of different radii and centres of curvature (the two values were kept within the certain ranges of proportion and sign relative to each other for each of the two lens boundaries which are necessary to simulate each kind of lens – for example, biconvex lenses require each centre of curvature to be on opposite sides of the lens, and for the radii of curvature to be sufficiently large for the circles to overlap).

The lens types investigated in this way were concave positive meniscus, plano-convex, convex-planar and both symmetrical and asymmetrical biconvex lenses. 3D plots of the aberration as a function of both radii and centres of curvature were then produced, and are shown in Figure 11.

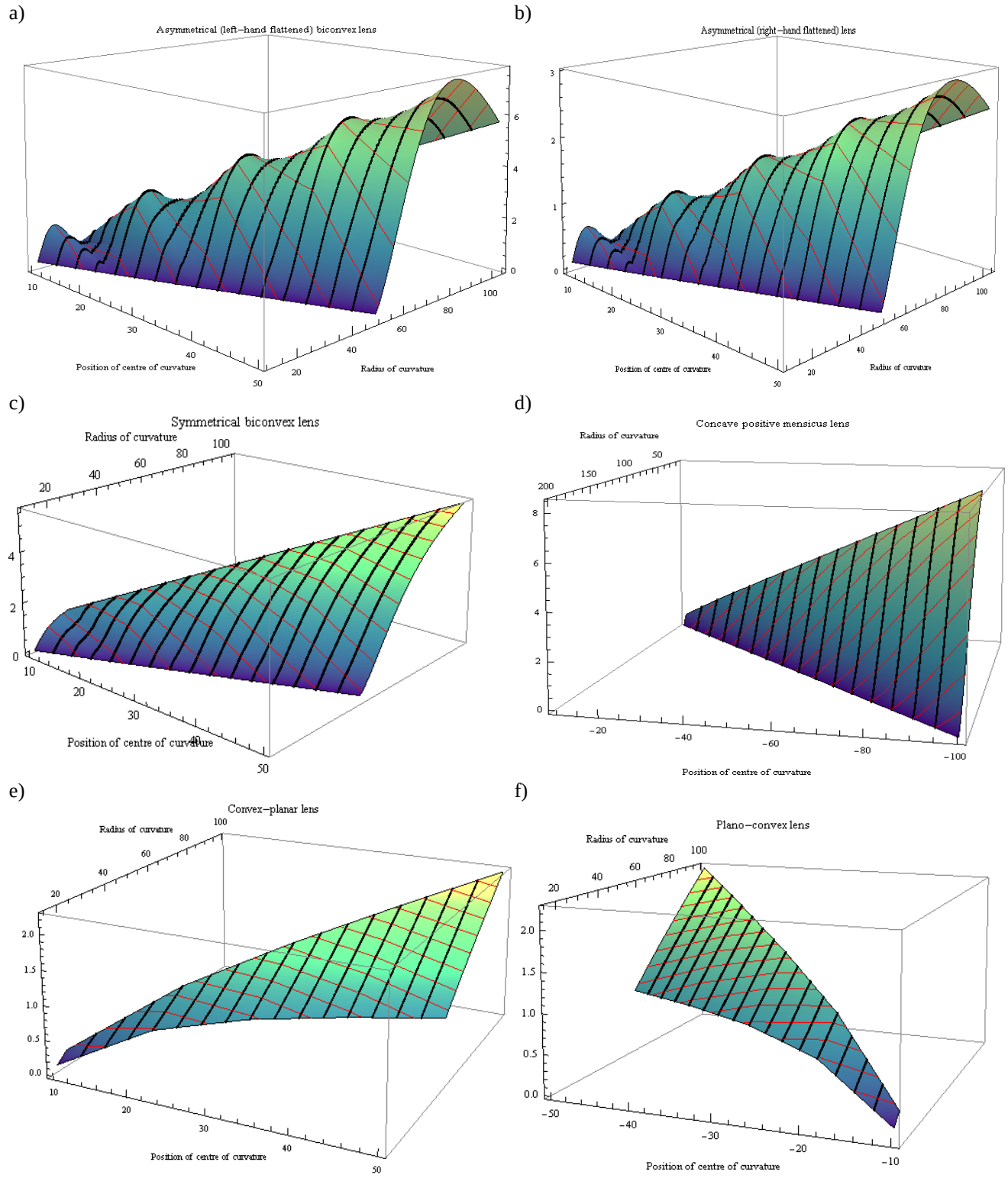

Figure 11: (a) Asymmetrical (left-hand flattened) biconvex lens. (b) Asymmetrical (right-hand flattened) biconvex lens. (c) Symmetrical biconvex lens. (d) Concave positive meniscus lens. (e) Convex-planar lens with flat face at x = 20. (f) Plano-convex lens with flat face at x = -20. Red lines are lines of constant radius of curvature; black lines are lines of constant position of the centre of curvature. The value of the measured spherical aberration for a modelled lens with some particular dimensions is given by the height of the plot at that point. Higher and lower regions are colour coded green and blue respectively. Electronic copies of these diagrams, which can be manipulated in 3 dimensions, are available from the URL included in the section "Further Work".

Spherical Aberrations

All plots demonstrate a general overall trend of rising aberration towards the corner of the plot with maximum radius of curvature and maximum distance of the centre of curvature from the origin. This is simply because in these cases the lenses are larger. Repeating patterns (for example, the ridges on the plots for the asymmetrical biconvex lenses) are due to the same series of variously proportioned lenses occurring multiple times, each time with different absolute sizes.

Figures 11(a), 11(b), 11(c) and 11(d), the three biconvex lenses and the convex positive meniscus lens, share the common characteristic that there is a line of almost zero aberration where the distance from the origin to the centre of curvature is almost equal to the radius of curvature, i.e. the thinnest lenses.

This extreme is not present in Figures 11(e) and 11(f) because neither the convex-planar nor the plano-convex lenses become extremely thin along this line, as the radius and centre of curvature of the flat side were kept constant at 10,020 and ±10,000 in order to approximate a flat surface at $x = \pm 20$ in the two cases. However, this region is still where the thinnest lenses are found and therefore where the measured aberration is at its lowest.

The convex-planar and plano-convex plots show a local maximum in the bottom corner. For a given radius of curvature, moving the position of the curved surface's centre of curvature to –20 (i.e. centring it on the flat surface, creating a hemispherical lens), maximises the aberration for that radius. This progression is illustrated in Figure 12.

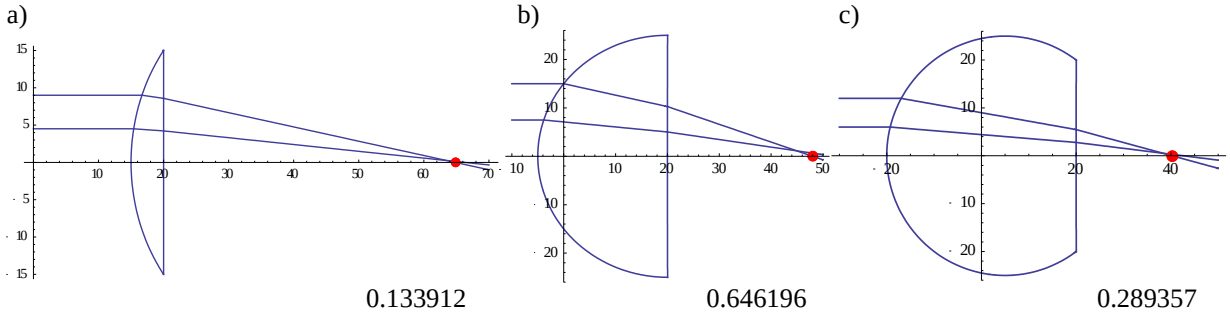

Figure 12: (a) A thin convex-planar lens from the right of the local maximum in Figure 11(e). (b) A hemispherical convex-planar lens from the local maximum in Figure 11(e). (c) A thick, more spherical convex-planar lens from left of the local maximum in Figure 11(e).

Both the left-hand flattened and right-hand flattened asymmetrical biconvex lenses show a steep rise in aberration as the dimensions of the lens move away from the line of extreme thinness, reach peak aberration in a state of relatively thick biconvexity, then, as the lenses move past this point they become more than half a sphere and aberration drops again as the rays are allowed to travel a greater distance through the glass and emerge closer together. This progression is illustrated in Figure 13.

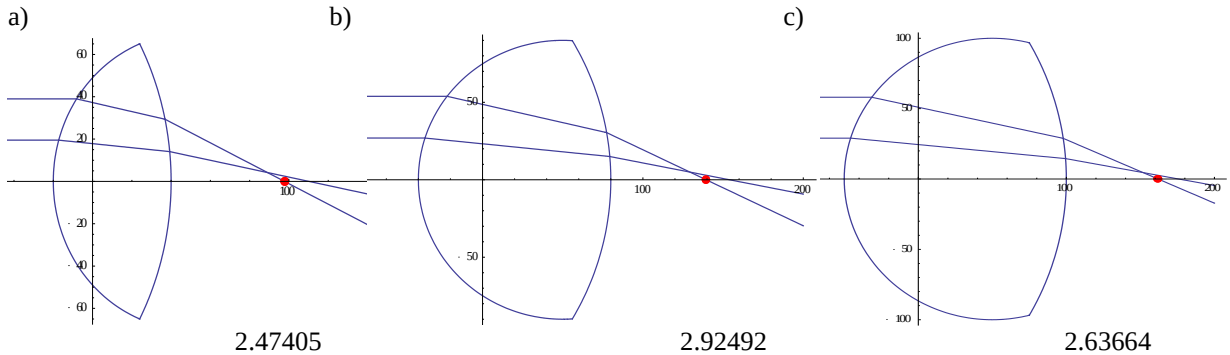

Figure 13: (a) A biconvex lens from the thin lens lower aberration region in Figure 11(b). (b) A thicker biconvex lens from the peak aberration region in Figure 11(b). (c) An even thicker biconvex lens from past the peak aberration region in Figure 11(c), causing the rays to emerge closer together.

The concave positive meniscus shows linear dependence of aberration with increasing dimensions, regardless of the ratios – for any given centre of curvature, reducing the radius of curvature will always make the lens thinner and reduce the aberration, and vice versa.

The symmetrical biconvex lenses exhibit a similar dependence, although it is not exactly linear. Because both lens faces are varied symmetrically, increasing the radius of curvature or decreasing the distance to the centre of curvature simply makes the lens thicker and increases the spherical aberration.

Comatic Aberrations (coma)

The same function used in Figures 6 and 7 to illustrate spherical aberrations with paraxial rays were re-used with a non-zero angle of elevation to find the types of coma produced by different lens shapes. Figure 14 demonstrates that symmetrical biconvex lenses as well as both concave and convex positive menisci produce negative coma.

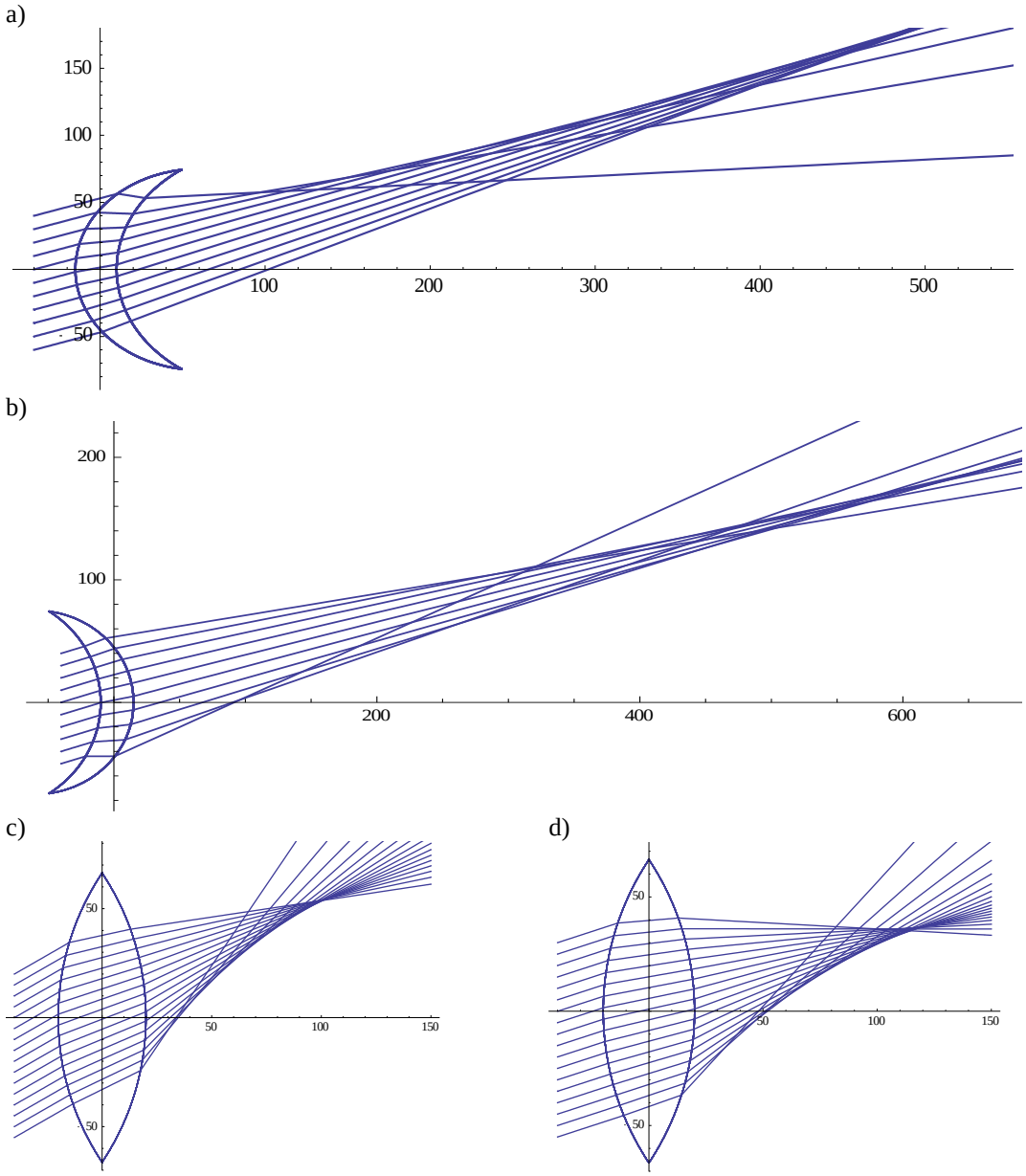

Figure 14: (a) A convex positive meniscus lens exhibiting negative coma. (b) A concave positive meniscus lens exhibiting negative coma. (c) A symmetrical biconvex lens with radii of curvature ±120 and a thickness of 40 subject to parallel rays at an angle of $\pi/6$, exhibiting weak negative coma. (d) The same biconvex lens subject to parallel rays at an angle of $\pi/10$.

Both positive meniscus lenses illustrated in Figures 14(a) and 14(b) show very significant negative coma. By contrast, the symmetrical biconvex lens in Figure 14(c) requires a large thickness and steep angle in order to exhibit noticeable (negative) coma. If it is subject to parallel rays at the same angle as the two menisci, as in Figure 14(d), the coma reduces to almost zero. Figure 15 shows the negative coma generated by a convex-planar lens and a plano-convex lens. It is concluded that all converging lenses simulated by the model demonstrate some negative coma, whether it is significant, as in the case of the menisci, or very slight as in Figure 14(d).

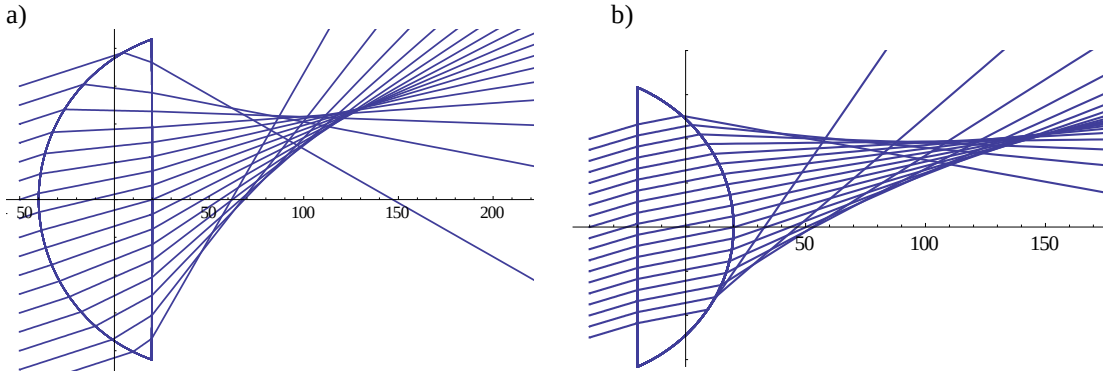

Figure 15: (a) A convex-planar lens exhibits negative coma. (b) A plano-convex lens exhibits slight negative coma.

Chromatic Aberrations

A solution was sought to the chromatic aberration produced by the symmetrical biconvex lens shown in Figure 9. As this lens was a converging lens (i.e. had a positive refracting power), a diverging (or negative) lens was needed in order to form an achromatic doublet. The behaviour of a Clark doublet was therefore investigated.

The specific design considered comprised of the biconvex borosilicate glass lens, with symmetrical radii of curvature ±217.7mm about centres at ±200mm, and a negative concave meniscus lens made of flint glass, with radii of curvature –217.7mm and –3819mm about centres at –200+*d* and –3790+*d*, where *d* is the distance in air between the two lenses. This formed the doublet, and its effect on the chromatic aberration is demonstrated in Figure 16.

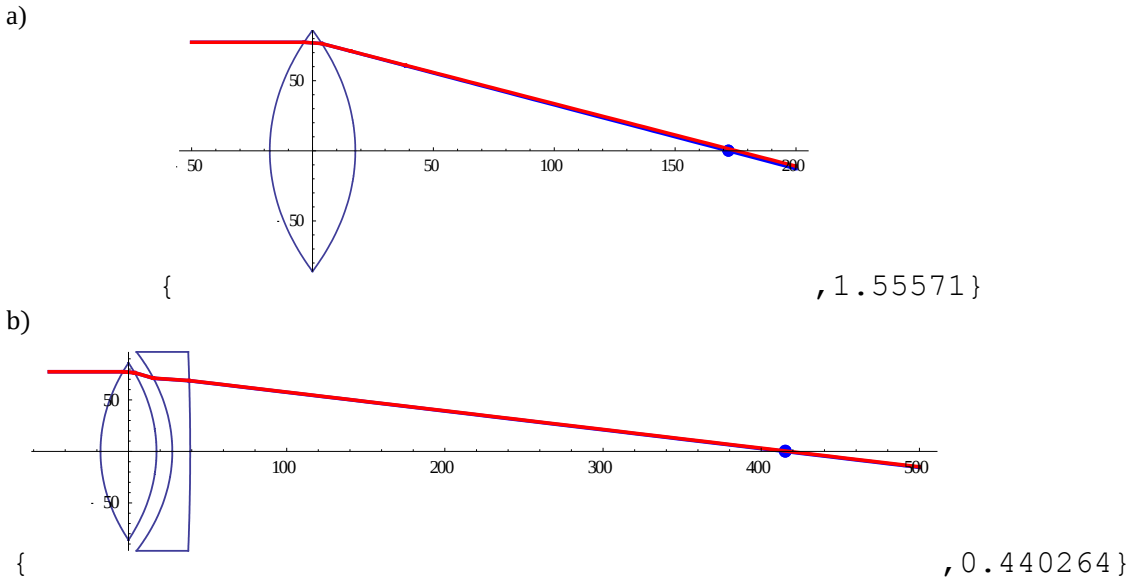

Figure 16: (a) Chromatic aberration of the borosilicate crown glass lens alone. (b) The Clark achromatic doublet results in significantly reduced chromatic aberration.

In order to find the lens spacing which produced the least chromatic aberration, the model's function for modelling the chromatic aberration of two lenses was supplied with a tabulated set of distances from 0mm to 20mm in increments of 1mm, in addition to the lenses' dimensions and their refractive indices for different coloured light: blue, red and yellow.

Since blue is the highest frequency colour of the three, the function was run twice, first comparing the foci of the red and blue ray and then comparing those of the yellow and blue ray, in order to determine the discrepancy between the rays in both cases. The absolute values of these differences were summed in order to describe the total chromatic aberration resulting from any particular distance between the two lenses.

A polynomial of order 10 was then fitted to this set (see Figure 17) and the minimum (over the range 0 to 20mm) was calculated, giving the lens separation which resulted in the least possible total chromatic aberration.

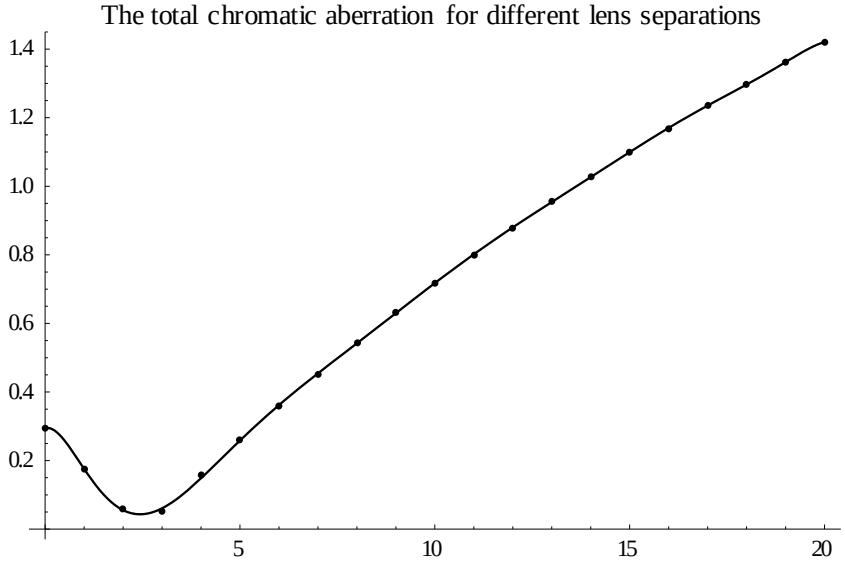

Figure 17: Plot of the total chromatic aberrations produced by the doublet as the distance between the two lenses varies from 0mm to 20mm (points) and the polynomial fit (line).

The lens separation which minimised the chromatic aberration was found to be 2.43433mm. When the lenses are this distance apart, the total chromatic aberration (that is, the sum of the distances of the yellow and red rays to the axis at the x-coordinate of the blue focus) was only 0.04081mm.

Maintaining the 3 equal radii of curvature of the doublet as constants, the larger radius of curvature of the flint glass' back face was then varied (about the same centre of curvature) from 3800mm to 4400mm in increments of 5mm, and the above routines were repeated to calculate, for each case, the optimal lens separation as well the minimum chromatic aberration that this separation produced, and these data were plotted over the range of distances. These plots are shown in Figures 18 and 19.

It should be noted that in the Cartesian sign convention, these radii would be considered negative, as the vertex of the curve is to the right of the centre of curvature, but for ease of implementation the functions use absolute values relative to the centre of curvature, and the plots display increasing radius to the right as this is the same direction in which the lens expands in Figure 16(b).

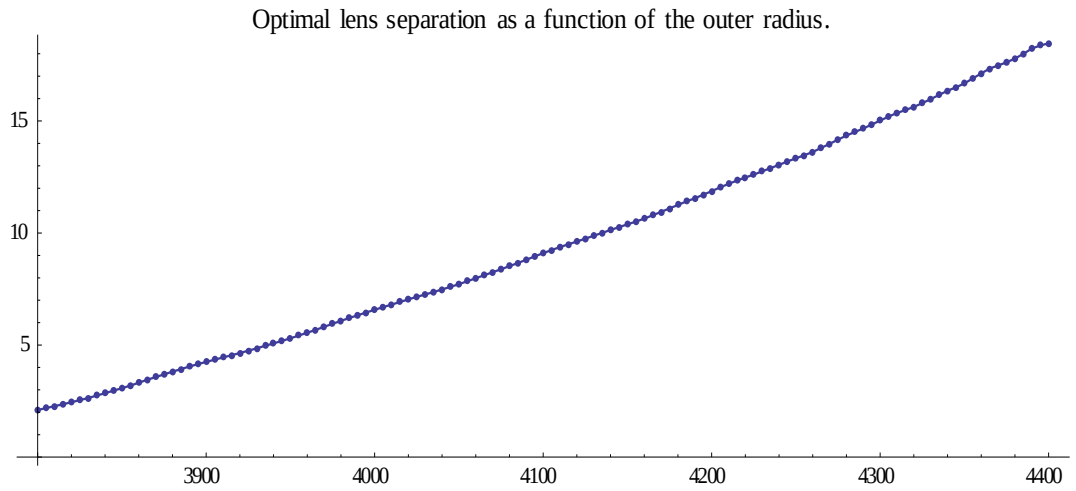

Figure 18: The optimal lens separation for different radii of curvature of the flint glass lens' back face.

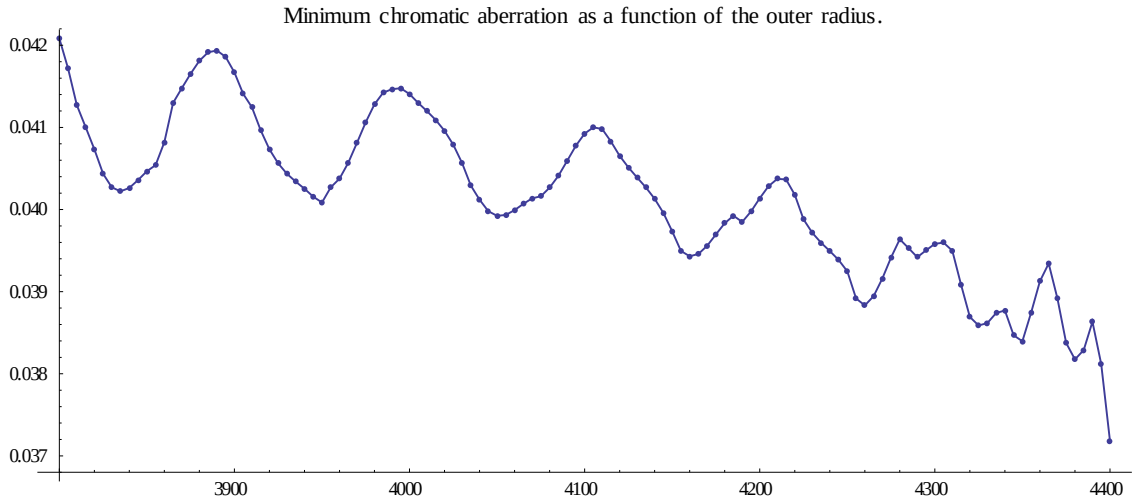

Figure 19: The minimum chromatic aberrations (i.e. those produced by the optimal lens separations shown in Figure 18) for each radius of curvature of the flint glass lens' back face.

It was found that, to minimise the chromatic aberration of the doublet as this radius was increased, the lenses have to be separated by a greater distance. For example, if the radius was 4000mm instead of 3819mm, it would be optimal to separate the lenses by 6.57276mm instead of 2.43433mm.

The relation between the minimum possible chromatic aberration with different radii shown in Figure 19 means that slightly altering the radius (and adjusting the lens separation accordingly) can reduce the chromatic aberration to a local minimum. However, each local minimum sits in a dip with a different shape, so an exact formula for finding these minima was not pursued.

Additionally, there is an overall trend that much larger radii have a tendency to produce slightly smaller minimum chromatic aberrations in general (these large radii produce very thick lenses in the model, as the distance centre of curvature of this outer face was only variable by up to 20mm).

To investigate this trend further, the model was used to calculate the optimum lens separation and chromatic aberration produced therewith for a range of back face radii of curvature from –2000mm to –105,000mm. In each case, the centre of curvature of the back face was adjusted to maintain a constant flint glass lens thickness of 10mm. The results of these calculations are shown in Figures 20 and 21.

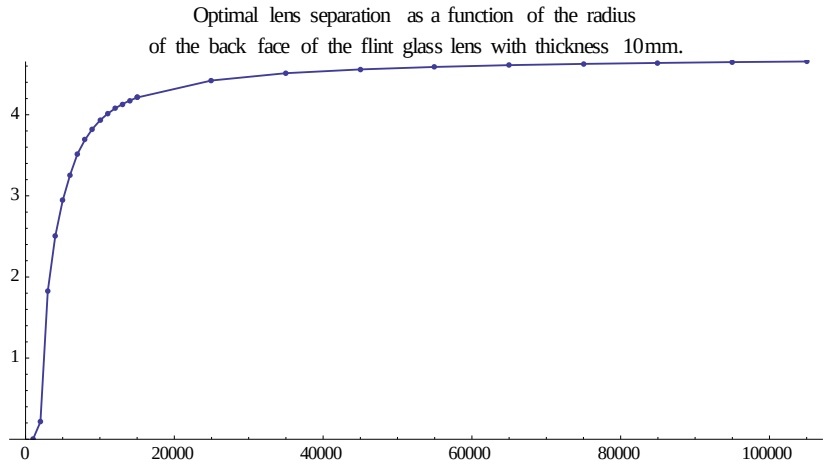

Figure 20: The optimal lens separation for the doublet using a flint glass lens of constant thickness 10mm with varying radius of curvature for its back face.

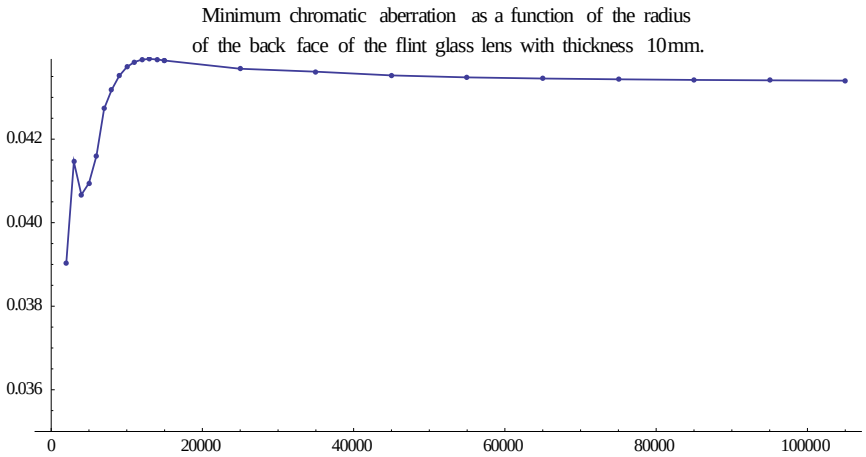

Figure 21: The minimum chromatic aberration produced by the doublet using a flint glass lens of constant thickness 10mm with varying radius of curvature for its back face.

As the radius of curvature of the flint glass lens' back face becomes extremely large this face becomes flat and the Clark doublet becomes a Littrow doublet. In this limit the optimal lens separation and the minimum possible chromatic aberration both tend to finite values.

These limits were determined by modelling an extremely large radius with order of magnitude 10^6 km to approximate an extremely flat lens. For the Littrow doublet, the optimum separation was found to be 4.7315mm, producing a minimum chromatic aberration of 0.0433458mm.

The plot in Figure 21 shows that the minimum possible chromatic aberration rises as the model moves from the Clark doublet to the Littrow doublet case, despite reaching a maximum value and then gradually reducing to its limiting value. A Littrow doublet with a flint lens thickness 10mm is therefore shown to be incapable of reducing chromatic aberrations to less than those produced by a Clark doublet using a flint glass lens of the same thickness.

Summary

Spherical Aberrations

The results of the model allow the following recommendations to be made for reducing spherical aberrations in particular types of lens:

- All lens types:
  Trivially, the thickness and overall size of the lens should be reduced, as the thinnest and smallest lenses produce the least significant spherical aberration.
- Convex-planar and plano-convex lenses:
  Hemispherical lenses should be avoided, as these produce the greatest spherical aberration. Moving past this to a thicker, more spherical lens will reduce the spherical aberration (demonstrated in Figure 12).
- Asymmetrical biconvex lenses:
  Biconvex lenses which are almost hemispherical with one side curved should be avoided. Using a rounder lens will reduce the spherical aberration (demonstrated in Figure 13).
- Concave positive meniscus and symmetrical biconvex lenses:
  Any alteration of one of the faces' radii and centres of curvature which reduces the lens' thickness will reduce the severity of the spherical aberration it produces.

Comatic Aberrations (Coma)

The coma produced by the following lens types were simulated by the model and found to be of a negative nature (i.e. generating a series of comatic circles with their tail pointing away from the axis of the lens):

- Convex positive meniscus lens
- Concave positive meniscus lens
- Symmetrical biconvex lens
- Convex-planar lens
- Plano-convex lens

The most significant examples of coma were produced by the positive meniscus lenses, relative to which all other investigated lens types showed only very slight negative coma (shown in Figures 14 and 15).

Chromatic Aberrations

The model was used to find the optimal distance between the two lenses forming an achromatic Clark doublet with the following composition:

- Symmetrical biconvex lens made of borosilicate glass, with symmetrical radii of curvature ±217.7mm about centres at ±200mm
- Concave negative meniscus lens made of flint glass, with radii of curvature –217.7mm and –3819mm about centres at –200+d and –3790+d, where d is the lens separation.

The optimum distance between these lenses was found to be 2.43433mm.

When the radius of the back face of the flint glass lens was varied, the optimum distance between lenses was found to increase as the radius did, i.e. when this radius is greater, making the second lens thicker and flatter, the flint glass lens should be positioned further away from the borosilicate glass lens.

The Clark doublet was smoothly transitioned into a Littrow doublet while maintaining a constant thickness, which showed that it was less effective at reducing chromatic aberration than the Clark doublet. It is therefore recommended that Clark doublets be favoured over Littrow doublets in terms of achromatism when the flint glass lenses have the same thickness.

Further work

This model can be used to simulate and examine other lens phenomena beyond those which have been explored here. To enable its re-use and modification, as well as to fully describe the methods used in this investigation (including the diagrams in Figure 11), a complete record of the *Mathematica* code defining the functions used by the model is available at:
www.homepages.ucl.ac.uk/~zcaph29/mathematica.html

Suggested areas for continued study are:

- The spike in the plot of chromatic aberration shown in Figure 21 (as the radius of curvature varies in the region below 10000) is not explained by the subsequent analysis in this report.
- The effect of the thickness of the flint glass lens on the plots in Figures 20 and 21 was not explored due in part to limitations on processing power. Given sufficient time, the model could be used to extend these 2D curves into a 3D surface over a range of thicknesses as well as radii of curvature.
- Other types of achromatic lenses which could be simulated by the model without requiring significant changes include Fraunhofer doublets, Steinheil doublets and Dialyte lenses.
- Other kinds of optical aberration (such as astigmatism) could be studied by a modified version of the model.